A Layer-Stripping Approach for Recovery of Scattering Media from Time-Resolved Data

Jenghwa Chang, Yao Wang#, Raphael Aronson
Departments of Electrical Engineering and Physics, Polytechnic University, Brooklyn, NY 11201

Harry L. Graber, Randall L. Barbour#
Departments of Pathology and Biophysics, SUNY Health Science Center, Brooklyn, NY 11203

Authors to whom inquiries should be addressed.

Abstract

This paper studies the reconstruction of the absorption properties of a dense scattering medium from time-resolved data. A Progressive Expansion (PE) Algorithm, similar to a layer-stripping approach, has been developed. The method progressively evaluates increasing depths within the medium by successively considering signals entering the detector at increasing times following an incident pulse. In order to reduce the propagation of reconstruction errors occurring at shallower depths, an overlapping scheme is introduced which uses readings from several consecutive time intervals in the reconstruction. In each overlapping time interval, the region under consideration is solved using a perturbation approach recently described by our group. The proposed algorithm is applied to several inhomogeneous media containing simple structures. Two sets of data have been tested: one calculated according to the perturbation model; and the other by Monte Carlo simulations. The results show that the PE method, when combined with proper overlapping, can make effective use of time-resolved data. Compared to our previous results with steady-state data, the present methods can probe deeper below the surface and produce a more accurate estimate.

1. Introduction

Recently a great interest has developed in recovering images, based on a tomographic measurement scheme, of tissues illuminated at near-infrared frequencies. At these frequencies, photons are intensely scattered. Several measurement schemes have been proposed as potentially suitable for interrogation of highly scattering media [1]. These include steady-state or time-independent [2], time-resolved [3-5], frequency modulated [6,7], and holographic schemes [8,9]. For dense scattering media involving thick structures, the intensity of the unscattered light rapidly becomes vanishingly small, leaving only the dominant diffusely scattered signal from which to attempt image recovery. In developing approaches to image reconstruction, our group has emphasized the first two of the four methods [10-14]. For many of the projected applications in acute-care medicine, we anticipate that only the backscattered field will be readily available. For this reason, reconstructed images reported here and elsewhere [10-14] have made use of only the backscattered field.

For imaging methods such as x-ray CT, in which the path of the detected signal is a straight line, the inverse problem can be accurately formulated as a system of linear equations of the form $\mathbf{A} = \mathbf{MX}$; where $\mathbf{A}$ is the measured response, $\mathbf{M}$ is the imaging operator and $\mathbf{X}$ is the unknown [15]. The form of this relationship is equivalent to Beer's law, which follows directly from the radiation transport equation in the limit of negligible scattering [16]. In the case of strong scattering, though, the change in photon intensity with distance becomes a non-linear function, because of the contribution of previously scattered photons which add to the net flux at a particular point and direction. A consequence of the additional term is that there is no generally applicable direct method for solving the inverse problem. One approach frequently applied to problems of this type is known as perturbation methods. This assumes that the composition of the unknown

0-8194-0940-5/92/$4.00

medium deviates only by a small amount from a known, reference medium. This approach is appealing, as it has the effect of reducing a highly nonlinear problem to one which is linear with respect to the difference between the target and reference media.

Over the past few years, our group has applied this strategy to develop methods for recovering the properties of dense scattering media by analyzing the backscattered fields using continuous [10-13] or time-resolved data [14]. The coefficients in the equations, referred to as weights, are the gradients of the detector readings with respect to the absorption properties of the points inside the medium [12,13]. For isotropically scattering media, the weight at a point for a given source-detector pair during a chosen time interval is the convolution of the forward and adjoint fluxes during that time at that point. Until now, we have attempted only one iteration of the perturbation approach using homogeneous media as references. In practice, calculation of the detector readings and weights for the current image estimate, which constitute the forward problem, was accomplished with Monte Carlo methods [13]. Several iterative reconstruction techniques - Projection Onto Convex Sets (POCS), Conjugate Gradient Descent (CGD), and a multi-grid reconstruction - were closely examined and compared [12]. The main difficulties in solving the problem reside in the extremely large number of unknowns, the noise characteristics of the data, and the underdetermined or ill-posed nature of the problem. Examination of the spatial distributions of weight functions reveals very steep gradients in weight with increasing depth. This has led us to explore the effect of varying the order in which data are incorporated into the calculation, with the result being that the proper sequence can have an effect analogous to layer stripping [13,14]. An improved version of the algorithm is reported here.

2. Reconstruction by Iterative Perturbation

The perturbation model for the steady-state case has been reported previously [12,13]. Here, we briefly describe the perturbation model for time-resolved data. Consider a measuring system where photons are injected with intensities S_j at J source locations ($j = 1, 2, \ldots, J$) on the surface of the test medium, and photon fluxes I_{jkl} are measured in L_{jk} time intervals ($l = 1, 2, \ldots, L_{jk}$) at the kth detector ($k = 1, 2, \ldots, K_j$) for the jth incident signal. In our study, collimated sources and detectors are used. The sources and detectors are placed on one side of the medium and the backscattered field alone is measured. Let the test medium be divided into N contiguous non-overlapping small volume elements, or voxels. The problem is to reconstruct the absorption coefficients x_i, $i = 1, 2, \ldots, N$, from the time-resolved measurements I_{jkl}. The perturbation model assumes that the absorption properties x_i of the unknown medium are very close to those of a reference medium, x_i^r. It relates the differences between the absorption properties of the two media, $\Delta x_i = x_i - x_i^r$, to the changes in detector readings, $\Delta I_{jkl} = I_{jkl}^r - I_{jkl}$, by the following first order approximation:

$$\sum_i w_{ijkl}\, \Delta x_i = \Delta I_{jkl},\ l = 1, 2, \ldots, L_{jk},\ k = 1, 2, \ldots, K_j,\ j = 1, 2, \ldots, J. \qquad (1)$$

Here, $w_{ijkl} = -\dfrac{\partial}{\partial x_i} I_{jkl}^r$ is called the *weight*, and specifies the reduction of the photon flux in time interval l at detector k due to the increase in absorption at voxel i when photons are injected from source j. The above equation can be represented in matrix form as

$$\mathbf{W}\,\Delta\mathbf{X} = \Delta\mathbf{I}\ . \qquad (2)$$

Given $\Delta\mathbf{I}$ and $\mathbf{W}$, $\Delta\mathbf{X}$ can be determined by solving the linear equation (2). Once $\Delta\mathbf{x}$ is found, $\mathbf{x}$ can be readily identified. When the reference medium is very different from the test medium, the approximation in Eq. (1) is inaccurate. Hence the above process should be repeated a number of times, with the reference image and the weight matrix being updated after each iteration. The process can be stopped when the difference between two successive estimates becomes smaller than a prescribed threshold. The calculation of the weights w_{ijkl} has been described in [14]. In this paper, we study the solution of the perturbation equation for a given reference medium and weight matrix.

3. Solving the Perturbation Equations

As mentioned previously, there are three principal difficulties in solving the perturbation equation. With regard to the problem of ill-posedness, a multi-grid progressive algorithm [12] has been developed for the steady-state case, which can reduce the number of unknowns so as to make the problem determined and reduce the computation time. The success of this method depends on the composition of the test medium and the way the coarse grids are formed. The low resolution image must satisfy a "local smoothness" property to produce reasonable results [17].

We have previously recognized that the gradient of weight as a function of depth is highly dependent on the temporo-spatial characteristics of the detector. We have consequently developed a layer-stripping algorithm which progressively evaluates the data in order of decreasing depth component of the weight gradients [13,14]. When applied to time-resolved data, this approach offers the additional advantage of reducing the number of unknowns and dimension of the weight matrix, thereby improving the determinedness and decreasing computation time. A difficulty with this approach is that reconstruction errors encountered early on tend to propagate and be amplified. A description of this scheme and an approach to reducing the propagation of errors is described in the next section.

3.1 A Progressive Expansion Algorithm for Time-Resolved Data

This algorithm makes use of the detector readings in different time intervals separately and in a progressive manner. In each time interval, we only consider the region which may contribute to the detector readings and which are not yet fixed from the previous reconstruction. The contribution to the detector readings in this time interval from the voxels solved earlier is first subtracted. The new unknowns are then solved based on the perturbation equation. Further, we assume that the reference image always has smaller absorption than the test medium, so that $\Delta x_i \geq 0$. This positivity constraint is applied to the reconstruction result after each time interval. More specifically, for a time interval t_l, the algorithm is as follows:

Step 1. Find all the detectors which may receive signal during t_l. This is accomplished by examining the weights of all the voxels for each detector. Only the detectors that have at least one non-zero weight associated with them are considered. The number of detectors found is here denoted as m_l. The set of detector indices is denoted by $\mathbf{I}_l$.

Step 2. Find all the non-fixed voxels which may contribute signal to any of the detectors determined in *Step 1*. This is accomplished by including all voxels which have non-zero weights for at least one of the selected detectors. The number of voxels found is here denoted by n_l. The set of voxel indices is denoted by $\mathbf{V}_l$.

Step 3. From the detector readings and voxels found in *Steps 1* and *2*, form the following set of linear equations:

$$\sum_{i \in \mathbf{V}_l} w_{ijkl}\ \Delta x_i \;=\; \Delta \mathrm{I}_{jkl} \;-\; \sum_{i \in \mathbf{V}_1, \ldots, \mathbf{V}_{l-1}} w_{ijkl}\ \Delta x_i\ , \quad j,k \in \mathrm{I}_l, \quad or \quad \mathrm{W}_l \Delta \mathrm{X}_l = \Delta \tau_l, \tag{3}$$

where $\Delta\tau_l$ consists of the detector readings minus the contribution from the voxels which are fixed in the previous reconstructions, $\Delta\mathbf{X}_l$ consists of the absorption increases in the voxels to be solved, and $\mathbf{W}_l$ is a m_l by n_l matrix composed of the weights of voxel i for detectors jk at time l, $i \in \mathbf{V}_l$, $jk \in \mathbf{I}_l$.

Step 4. Find the least squares solution of Eq. (3) for $\Delta x_i \in \mathbf{V}_l$. In our study, the CGD method is used for its relatively fast convergence.

Step 5. Apply the positivity constraint to the reconstructed values. This is accomplished by setting $\Delta x_i = 0$ if $\Delta x_i < 0$.

Step 6. Fix $\Delta x_i \in \mathbf{V}_l$. Go to the next time interval.

3.2 An Overlapping Scheme

In the algorithm described above, a voxel is solved and fixed when its signal is first detected by some detectors. Since the weight of this voxel at this initial time is usually small, the reconstruction is not reliable. The error in this voxel will further affect the reconstruction of other voxels at later times.

In order to overcome this problem, an overlapping scheme has been developed. In this method, a voxel is not fixed the first time it is solved. Rather, it is considered in the next several time intervals. In each time interval, new voxels that first contribute signals in this time interval as well as certain old voxels are considered. After the solution of the perturbation equation involving all those voxels, a partial set of the old voxels (those that have been considered in the most previous time interval) are fixed. And the next time interval is considered. This overlapping scheme can greatly reduce the propagation of reconstruction error in the proposed PE algorithm and provide more reliable reconstruction. However, it also leads to several problems. First, the early detected signals are more ballistic and contain information that is not merged with scattered signals from other voxels too much. Overlapping will lessen the influence of this kind of information in the final result. Second, overlapping will increase the number of unknowns to be solved in each time interval and consequently the computation time. Too much overlapping may even make the problem underdetermined at some early time intervals, which will make the reconstruction in the following intervals less reliable. If we overlap many time intervals at once, the reconstruction problem will become similar to that in the steady-state case. Therefore, we need to select the overlapping interval properly to arrive at a good compromise.

4 Results

In this section, we show reconstruction results for test media with different absorption distributions. They were obtained by the PE algorithm running on the Kilonode parallel computer [18].

4.1 Media Containing Point Absorbers

To evaluate the capability of the proposed reconstruction method to resolve absorption distributions at different depths from backscattered measurements alone, we have attempted the reconstruction of one or two closely juxtaposed point absorbers of size 1 mfp^3 buried at various depths in an isotropically scattering half-space. The absorption coefficient of the background medium is 1 % of the total cross-section, and that of the absorber is 5 %. Only a volume of size 41x41x10 mfp^3 is considered, with a total of 16,810 unit-size voxels. The source is positioned at the center of the surface of the medium and detectors are uniformly distributed on the surface, separated by 1 mfp along each direction, with a radius of 10 mfp. The same medium without absorbers is chosen as the reference. The differences in detector readings for several absorber configurations are generated directly according to Eq. (1). Gaussian noise was added to the readings to evaluate the noise sensitivity of the algorithm. The ratio of the noise variance to the mean value of the difference in detector readings is used as the measure of noise level.

Reconstruction results for the media containing a single point absorber at depth 1-2 and 4-5 mfp, respectively, are presented in Figs. 1(a)-1(d) and 2(a)-2(d). In all the figures, the gray level represents the relative increase in absorption over the reference media. The degree of darkening is proportional to the relative increase. For display purposes, the images have been scaled to the same minimum and maximum darkness. Hence, the same gray level in separate figures may represent different absorption levels. The existence of the absorber is clearly revealed in both cases. The left and right panels are the Y-Z and X-Z cross-sections of the media, respectively. Figs. 1(a) and 2(a) show the original media. Figs. 1(b) and 2(b) are the reconstructed images, using data corresponding to photons having traveled a total distance of between 1 and a maximum of 20 mfp using a time interval of 1 mfp (i.e., 0-1, 1-2, ..., 19-20), without overlapping. Figs. 1(c)-1(d) and 2(c)-2(d) compare reconstructed images from data with added noise, with and without overlapping. It can be seen that overlapping produces a higher quality image. Further, a comparison of Figs. 1(d) and 2(d) reveals that at deeper layers, the reconstructed image is more sensitive to noise. It should be noted that most of the image artifacts seen at locations away from the central axis of the source would be expected to vanish had additional source positions been considered. Reconstructed images at different noise levels for the medium containing a point absorber at 1-2 mfp are

presented in Figs. 3(a)-3(d). As expected, the reconstruction quality is worsened as the noise level increases, but the result at the 20% noise level is still quite reasonable. Figs. 4 and 5 show the results for two point absorbers separated by 1 mfp at depths 1-2 and 4-5 mfp, respectively. The results are similar to the single absorber case - overlapping significantly outperforms the non-overlapping case and deeper layers are more sensitive to noise.

4.2 A "T" Absorber Medium

The above results are based on calculated data. In this section, we present reconstruction results from data obtained by calculation as well as from Monte Carlo simulations for an isotropically scattering medium containing a "T" shaped black absorber. Two orthogonal cross-sections of the actual "T" absorber medium are shown in Fig. 6(a). The left and right columns are the Y-Z and X-Z cross-sections of the medium, respectively. For calculated data the source-detector configurations are the same as the point-absorber case. For the simulated data the source configuration is shown in Fig. 7(b); two detector configurations, shown in Figs. 8(a) and 8(b), were used. Only detectors oriented normal to the medium were used, to limit required computation time.

Fig. 6(b) shows the result by the PE algorithm based on calculated data. The reconstructed image has a sharp transition at the top region of the "T" but there is evidence of image degradation at greater depths. This is due to numerical errors as well as to the propagation of reconstruction error. Figs. 6(c) and 6(d) show images reconstructed from the same simulation data but employing two different detector distributions, shown respectively in Fig. 8(a) and 8(b). The poor result seen in Fig. 6(c) is a consequence of employing a set of readings with too great a spacing between the detectors. When the denser packing of detectors was used, a much better result was obtained, in which the top two layers ("cap") of the "T" were reconstructed quite accurately but the lower portion ("stem") was smeared. Note that the changes in detector readings in the presence of such a large black absorber will not follow the perturbation model accurately. Nevertheless, the reconstructed image based on this model contains a sharp darkening in the region where the "T" absorber is located. This is a very encouraging result, as it suggests that even with a reference medium that is quite different from the real medium, one iteration of the perturbation method may yield useful results.

4.3 A Three-Layer Medium

Fig. 9 shows the reconstruction result for a 3 layer medium from simulated data. The original medium is shown in Fig. 9(a). It is 10 mfp thick, and the three layers are located in depth 0-3, 3-7, and 7-10 mfp, respectively. The absorption coefficient of the first and third layers is 1%, and that of the middle layer is 5%. The sources are uniformly distributed on the surface, separated by 1 mfp along each direction within a area of 17x17 mfp^2, and the detector configuration is shown Fig. 8(c). A homogeneous medium with an absorption value of 1% of the total cross-section is used as the reference. The reconstruction reveals correctly, with slight blurring, the three-layer structure. The transition from the first to second layers was correctly reconstructed and the transition from the second to third was less accurate. The absorption level of the second layer is overestimated and its thickness is underestimated. This is as expected, since the weights used in the voxels in the second and third layers are much larger then the actual weights.

5 Discussion

To the best of our knowledge, the current study and another recently reported [14] are the first to attempt time-resolved 3-D tomographic reconstruction of the subsurface structure of dense scattering media based on remote sensing measurements. Our approach has been to solve the inverse problem of the radiation transport equation, in the case of elastic, isotropic scattering, by employing a perturbation approach. Because the transport equation represents a general expression valid over a range of photon energies and of target medium structures, the scheme we have described may well be applicable to a broad range of other imaging applications.

A principal difficulty encountered when dealing with highly diffused signals is that invariably the inverse problem is both ill-conditioned and ill-posed. One consequence of this is to greatly increase the size of the computation, especially if a 3-D reconstruction is sought. This, in itself, can introduce added complexity, for as the problem size grows it becomes increasingly important to adopt computing strategies that minimize the communication overhead among the computing

nodes [18]. To date, we have explored two strategies in an effort to minimize these difficulties. One has been to employ algorithms that allow us to improve the conditioning of the problem, either by inclusion of additional information (e.g., use of POCS [12]) or by reducing the number of unknowns through a multi-grid scheme. The second has been to incorporate detector readings in a sequence that makes use of knowledge of the underlying physics of photon transport in random media. That is, the existence of a steep weight gradient permits the implementation of analysis schemes that have the effect of layer-stripping. The results reported earlier [12,13] have demonstrated that acceptable image quality can be obtained even in the case of steady-state measurements, which ought to be the most problematical because there is non-zero weight in all voxels. In practice, the very rapid reduction in weight with increasing depth has the effect of guiding the algorithm to solutions close to the correct one even through the problem may be underdetermined. The observation that recognizable images can be obtained based on time-independent measurements is consistent with reports by Singer *et al.* [19] and Grunbaum *et al.* [20].

By introducing temporal resolution, the conditioning of the problem is improved, as at early time intervals extensive regions having zero weight may exist. As mentioned above, though, a potential difficulty in employing a layer-stripping scheme is the propagation of reconstruction errors. This problem can be addressed, at least partially, by implementing the described overlapping scheme. Choosing the correct time interval in which to fix a voxel, when using the overlapping PE algorithm, involves a balancing of two opposing trends. The first is that as time increases the detector readings contain information about an increasing number of voxels; for this reason it would appear desirable to fix the absorption coefficient of each voxel as early as possible. The second is that a voxel's weight is a function of time, initially very small and increasing to a maximum value at a time that is usually considerably larger than that taken by light traveling from source to voxel to detector in straight lines. The estimate of the absorption in a given voxel consequently can not be fixed with confidence until after the time of peak weight has passed for many of the source-detector pairs considered in the reconstruction. This accounts for the improved results of the overlapping PE compared to the simple PE algorithm; additional improvement is expected when more sophisticated "fix time vs. voxel location" procedures are implemented.

Because of the progressive nature of the PE algorithm, error propagation is more serious as the region grows deeper since the weights of the voxels in the previous regions generally are intrinsically higher than those in the later one. The error propagated from the previous voxels will be amplified by their relatively larger weights. This, as well as the numerical error, may set a limit on the depth to which the algorithm can provide reliable reconstruction. Methods for reducing error propagation as well as analysis of the limit of this algorithm by this error are very important and need further investigation.

Finally, it is useful to consider the feasibility of implementing the proposed scheme in relation to alternate approaches being considered [21]. As with any imaging scheme, acquisition of data with a high S/N ratio is important. Arridge *et al.* [21,22] have suggested use of the mean value of the temporal profile rather than evaluation of discrete time intervals, as the former will provide a more stable signal. Our analysis, on the other hand, has made use of the earliest time intervals available, as these signals have experienced the least amount of scattering. While the S/N ratio corresponding to this data may generally be less than for a mean time of flight value, the information content should be greater as the latter constitutes an averaging effect. Clearly, efforts to probe to greater depths will require evaluation of longer time intervals, especially in the backscattering mode. As discussed above, this acts to rapidly increase the dimension of the problem. We have shown here, however, that an overlapping approach improves the conditioning of the problem and extends the depth to which an accurate reconstruction can be achieved.

Recently, several groups have emphasized the possibilities of frequency-domain schemes [6,7] for the imaging problem. Since the phase shift is related to the mean photon transit time [7], this method may represent a more practical approach, as the cost and complexity of this scheme is currently less than that of time-resolved measurements. It is important to recognize that phase shift measurements at a given frequency have an uncertainty of $2n\pi$, likely rendering solutions to the inverse problem nonunique.

References

[1] B. Chance, "Optical method," *Ann. Rev. Biophys. Biophys. Chem.* 20:1-28, 1991.

[2] K.M. Yoo, G.C. Tang, and R.R. Alfano, "Coherent backscattering of light from biological tissues," *Appl. Opt.* 29:

3237-3239, 1990.

[3] L. Wang, P.P. Ho, C. Liu, G. Zhang, and R.R. Alfano, "Ballistic 2-D imaging through scattering walls using an ultrafast optical Kerr gate," *Science* 253:769-771, 1991.

[4] J.C. Hebden and R.A. Kruger, "A time-of-flight breast imaging system: spatial resolution performance," in *Proc. Time-Resolved Spectroscopy and Imaging of Tissues*, SPIE-1431, pp. 225-231, 1991.

[5] B. Chance *et al.*, "Comparison of time-resolved and -unresolved measurements of deoxyhemoglobin in brain," *Proc. Nat. Acad. Sci.* 85:4971-4975, 1988.

[6] J. Fishkin, E. Gratton, M.J. vandeVen, and W.W. Mantulin, "Diffusion of intensity modulated near-infrared light in turbid media," *SPIE*-1431, pp. 122-135, 1991.

[7] E.M. Sevick, B. Chance, J. Leigh, S. Nioka, and M. Maris, " Quantitation of time- and frequency- resolved optical spectra for the determination of tissue oxygenation," *Anal. Biochem.* 195:330-351, 1991.

[8] K.G. Spears, J. Serafin, N.H. Abramson, X. Zhu. and H. Bjelkhagen, "Chrono-coherent imaging for medicine," *IEEE Trans. Biomedical Eng.* 36:1210-1221, 1989.

[9] A. Rebane and J. Feinberg, " Time-resolved holography," *Nature* 351:378-380, 1991.

[10] R.L. Barbour, H. Graber, R. Aronson, and J. Lubowsky, "Model for 3-d optical imaging of tissue," in *Proc. 10th Annual Int. Geoscience and Remote Sensing Symposium*, vol. II, pp. 1395-1399, IEEE Press, 1990.

[11] R. Aronson, R.L. Barbour, J. Lubowsky, and H. Graber, "Application of transport theory to infrared medical imaging," in *Modern Mathematical Models in Transport Theory; Advances and Applications* 51:64-75, Birkhauser Press, 1991.

[12] Y. Wang, J. Chang, R. Aronson, R.L. Barbour, H.L. Graber, and J. Lubowsky, "Imaging Scattering Media by Diffusion Tomography: An Iterative Perturbation Approach," in *Proc. Physiological Monitoring and Early Detection Diagnostic Methods*, SPIE-1641, (Los Angeles), pp. 58-71, Jan. 1992.

[13] R.L. Barbour, H.L. Graber, R. Aronson, and J. Lubowsky, "Imaging of subsurface regions of random media by remote sensing," in *Proc. Time-Resolved Spectroscopy and Imaging of Tissues*, SPIE-1431, (Los Angeles), pp. 192-203, Jan. 1991.

[14] R.L. Barbour, H.L. Graber, R. Aronson, and J. Lubowsky, " Imaging of diffusing media by a progressive iterative backprojection method using time-domain data," in *Proc. Physiological Monitoring and Early Detection Diagnostic Methods*, SPIE-1641, (Los Angeles), pp. 21-34, Jan. 1992.

[15] A.C. Kak and M. Slaney, *Principles of Computerized Tomographic Imaging*, IEEE Press, 1988.

[16] A. Ishimaru, *Wave Propagation and Scattering in Random Media*, Chapter 7, Academic Press, 1978.

[17] T.S. Pan and A.E. Yagle, " Numerical study of multigrid implementation of some iterative image reconstruction algorithms," *IEEE Trans. Medical Imaging*, MI-10:572-588, 1991.

[18] F.H. Schlereth, J.M. Fossaceca, A.D. Keckler, and R.L. Barbour, "Imaging in diffusing media with a neural net formulation: A problem in large scale computation," in *Proc. Physiological Monitoring and Early Detection Diagnostic Methods*, SPIE-1641, (Los Angeles), pp. 46-57, Jan. 1992.

[19] J.R. Singer, F.A. Grunbaum, P. Kohn and J.P. Zubelli, "Image reconstruction of the interior of bodies that diffuse radiation," *Science*, 248:990-993, 1990.

[20] F.A. Grunbaum, P. Kohn, G.A. Latham, J.R. Singer, and J.P. Zubelli, "Diffuse tomography," in *Proc. Time-Resolved Spectroscopy and Imaging of Tissues*, SPIE-1431, pp. 232-238, Jan. 1991.

[21] S.R. Arridge, M. Cope, D.T. Delpy, " The theoretical basis for the determination of optical pathlengths in tissue: temporal and frequency analysis," *Phys. Med. Biol.* 37:1531-1560, 1992.

[22] S.R. Arridge, P. van der Zee, M. Cope, and D.T. Delpy, "Reconstruction methods for infra-red absorption imaging," in *Proc. Time-Resolved Spectroscopy and Imaging of Tissues*, SPIE-1431, pp. 204-215, 1991.

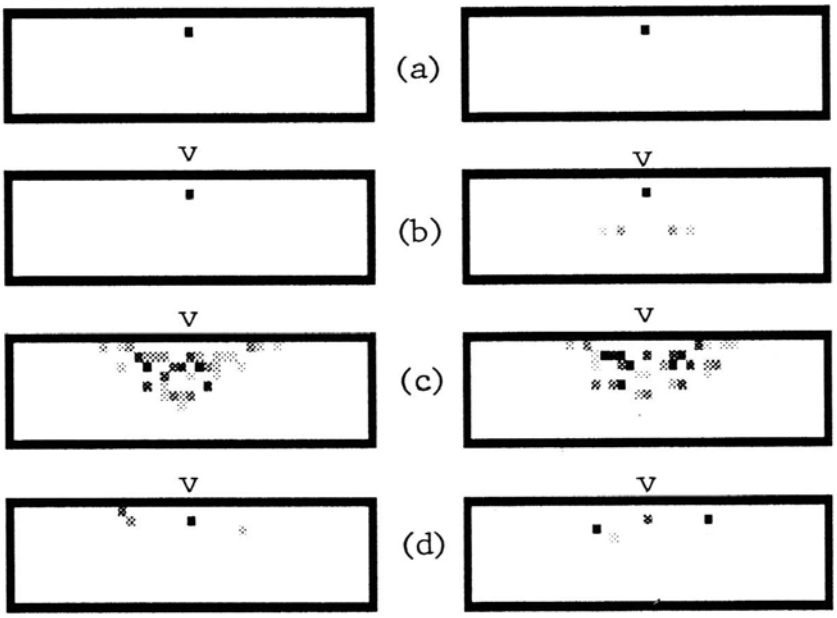

Fig. 1. Reconstruction of the medium containing a point absorber at depth 1-2 mfp, from calculated data. The source configuration is as shown in Fig. 7(a). The detectors are uniformly distributed on the surface in a grid-like manner separated by 1 mfp in each direction. The images on the left side show the Y-Z cross section and those on the right the X-Z cross section. (a) Original. (b) Reconstruction from noiseless data without overlapping. (c) Reconstruction from noise-added data without overlapping. The noise level is 2%. (d) Reconstruction from noise-added data with an overlapping interval of 3 mfp. All the reconstruction results are obtained by considering data corresponding to photons having traveled a distance between 1-12 mfp using a time interval of 1 mfp. Images shown were thus limited to within an hemisphere of 6 mfp originating from the position of the photon entry. "v" indicates location of source.

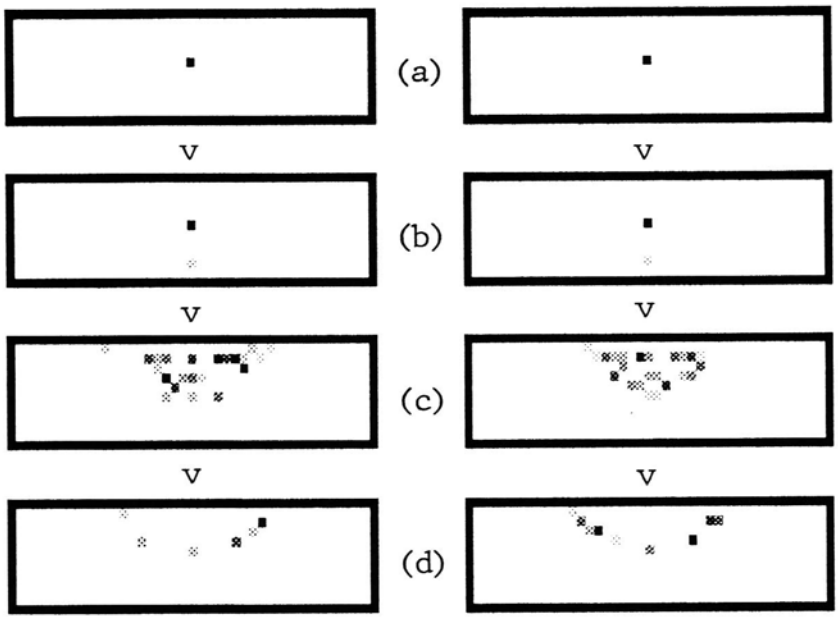

Fig. 2. Reconstruction of the medium containing a point absorber at depth 4-5 mfp, from calculated data The source and detector configurations are the same as in Fig. 1. (a) Original. (b) Reconstruction from noiseless data without overlapping after 20 time windows of width 1 mfp (i.e., 0-1, 1-2, ..., 19-20). (c) Reconstruction from noise-added data without overlapping. The noise level is 10%. (d) Reconstruction from noise-added data with an overlapping interval of 3 mfp. The results in (b), (c) and (d) are limited to within hemispheres of 10, 6 and 5 mfp originating from the point of photon entry respectively. "v" indicates location of source.

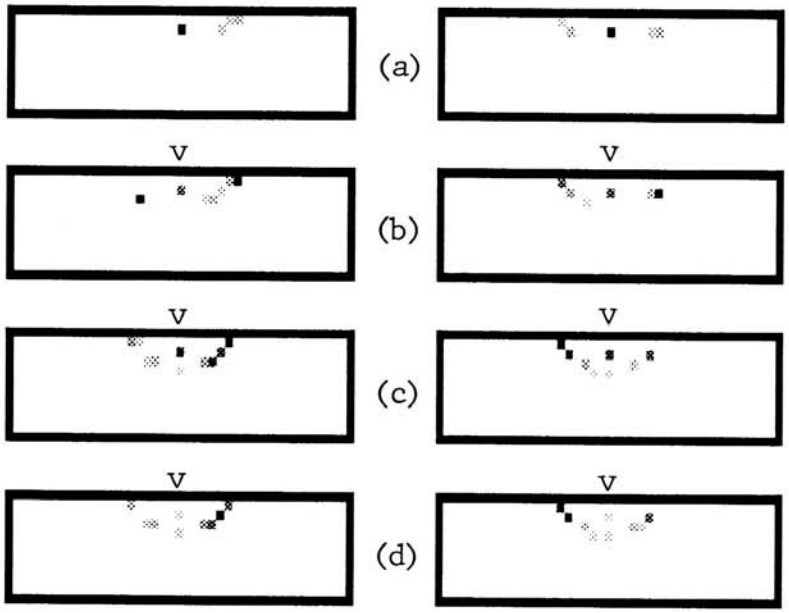

Fig. 3. Reconstruction of the medium in Fig. 1(a) at different noise levels. The noise levels are respectively (a) 1%, (b) 5%, (c) 10%, and (d) 20%. All the reconstruction results are obtained with an overlapping interval of 3 mfp after 12 time windows of width 1 mfp (i.e., 0-1, 1-2,..., 11-12). Volume of medium considered in the reconstructed image is the same as in Figure 1. "v" indicates point of photon entry.

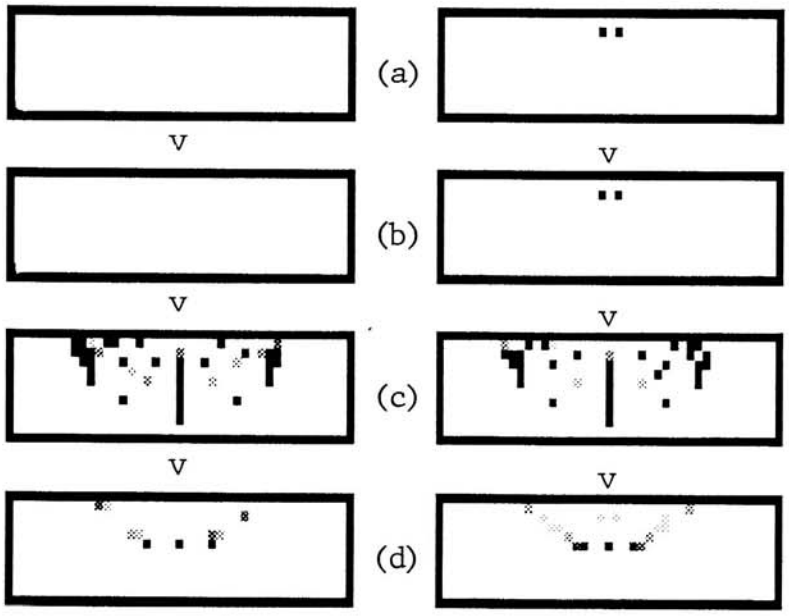

Fig. 4. Reconstruction of the medium containing two point absorbers separated by 1 mfp at depth 1-2 mfp, from calculated data. The source and detector configurations are the same as in Fig. 1. (a) Original. (b) Reconstruction from noiseless data without overlapping. (c) Reconstruction from noise-added data without overlapping, the noise level is 2%. (d) Reconstruction from noise-added data with an overlapping interval of 3 mfp. All the reconstruction results are obtained after 14 time windows of width 1 mfp. The results in (b), (c) and (d) are limited to within hemispheres of 10, 7 and 6 mfp originating from the point of photon entry, respectively. "v" indicates location of source.

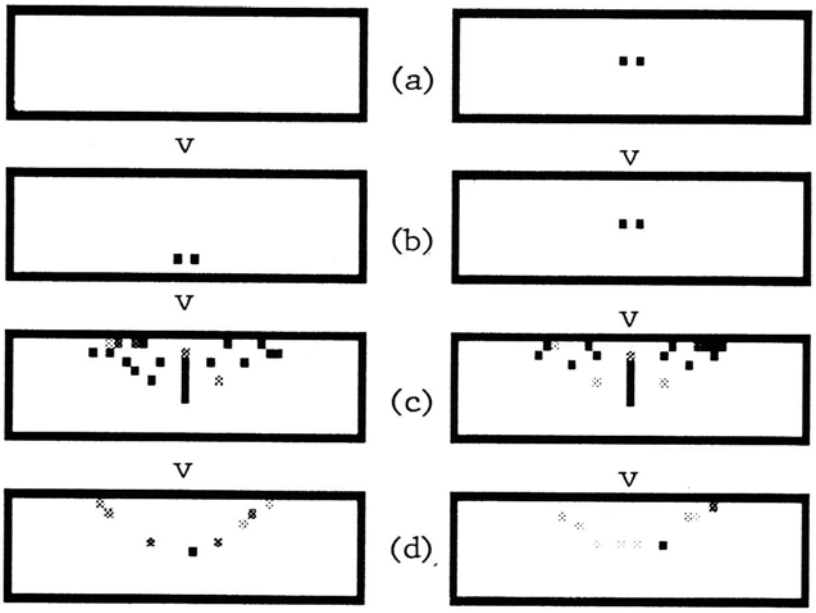

Fig. 5. Reconstruction of the medium containing two point absorbers separated by 1 mfp at depth 4-5 mfp, from calculated data. The source and detector configurations are the same as in Fig. 1. (a) Original. (b) Reconstruction from noiseless data without overlapping after 20 time windows of width 1 mfp. (c) Reconstruction from noise-added data without overlapping, the noise level is 10%. (d) Reconstruction from noise-added data with an overlapping interval of 3 mfp. The result in (c) and (d) are both obtained after 14 time windows. Volume of medium considered in the reconstructed image is the same as in Fig. 4. "v" indicates location of source.

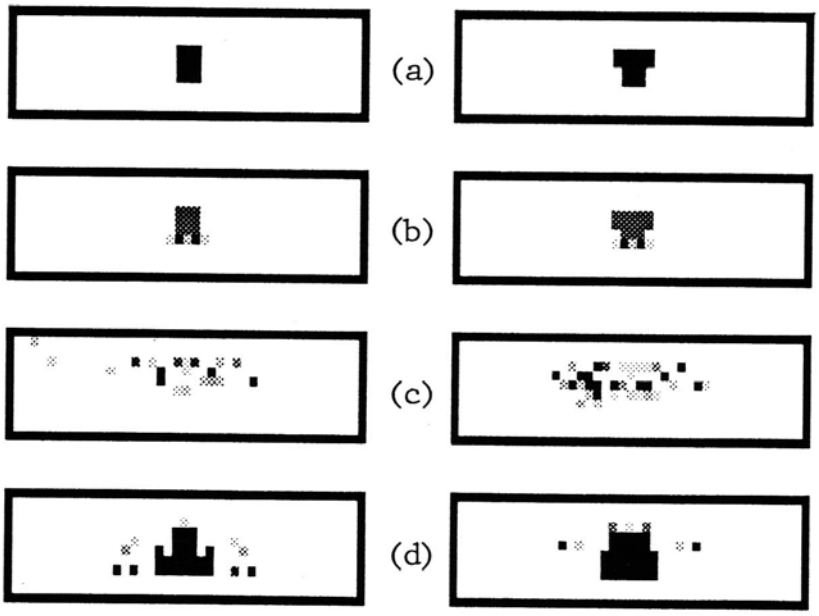

Fig. 6. Reconstruction of the medium containing the "T" absorber from calculated and simulated data. (a) Original. (b) Reconstruction from calculated data after 16 time windows of width 1 mfp (i.e., 0-1, 1-2, ..., 15-16) without overlapping. The source and detector configurations are the same as in Fig. 3. (c) Reconstruction from Monte Carlo simulated data after 9 time windows of width 2 mfp (i.e., 0-2, 2-4, ..., 16-18) with an overlapping interval of 2 mfp. The source and detector configurations are as shown in Figs. 7(b) and 8(a), respectively. (d) The same as in (c), except that the detector configuration is as shown in Fig. 8(b).

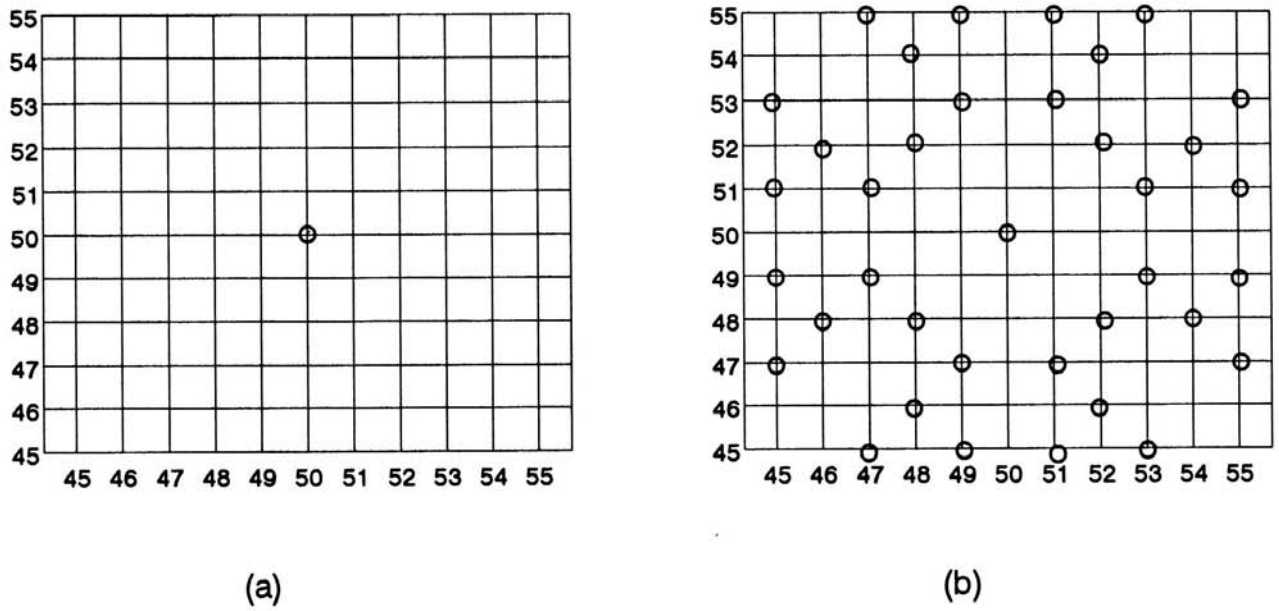

Figure 7. (a) Source configuration for calculated data – a single source at the center; (b) Source configuration for simulated data of the "T" absorber.

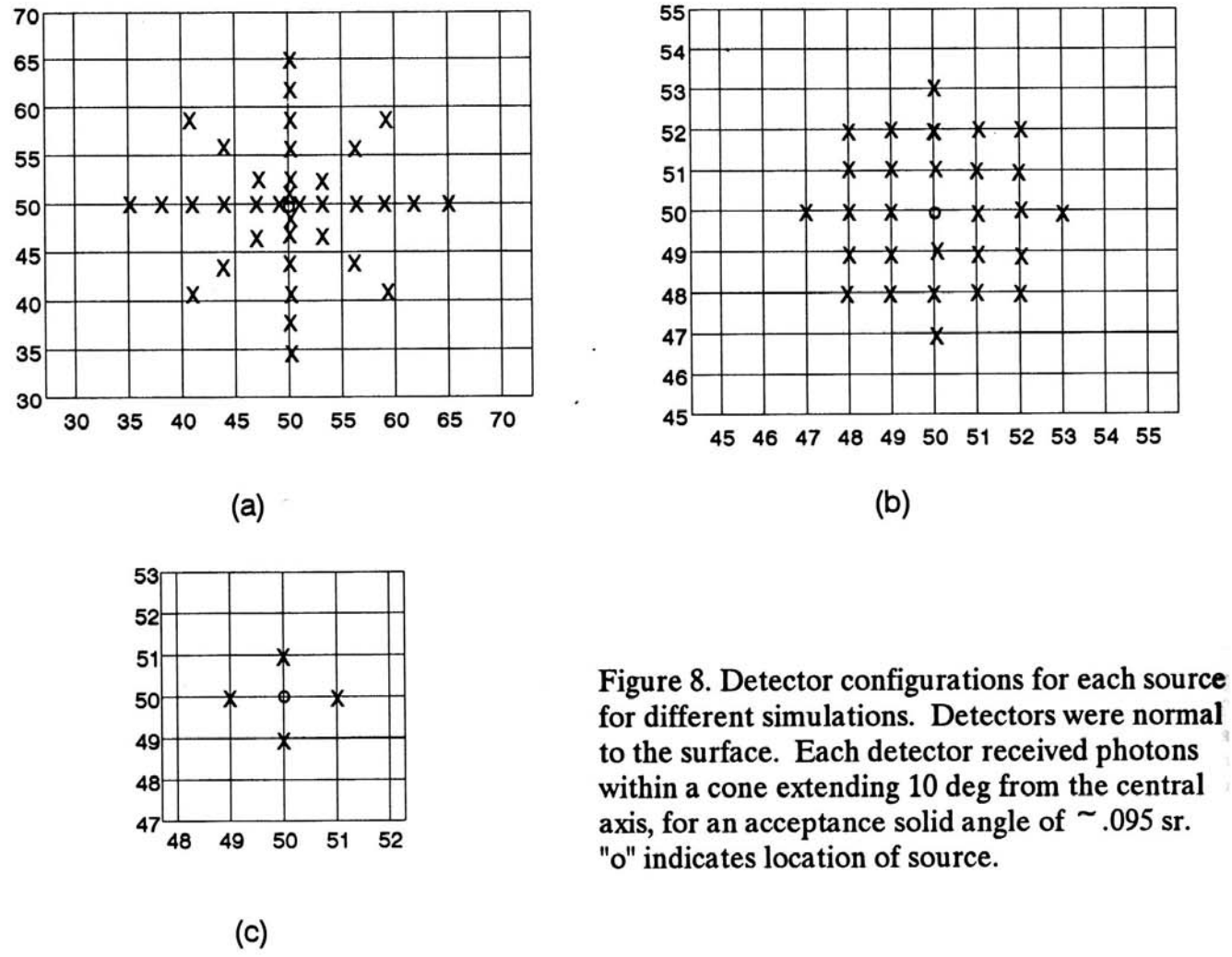

Figure 8. Detector configurations for each source for different simulations. Detectors were normal to the surface. Each detector received photons within a cone extending 10 deg from the central axis, for an acceptance solid angle of ~.095 sr. "o" indicates location of source.

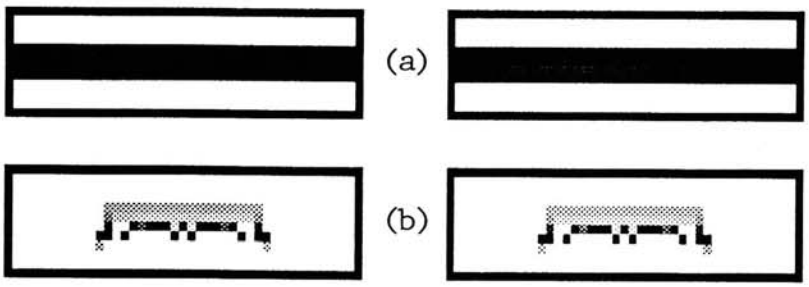

Fig. 9. Reconstruction of the three-layer medium from simulated data. (a) Original. (b) Reconstruction from Monte Carlo simulation data after 10 time windows of width 2 mfp (i.e., 0-2, 2-4, ..., 18-20) with an overlapping interval of 2 mfp. The sources are located uniformly over a 17x17 mfp^2 region in a grid-like manner separated by 1 mfp in each direction. The detector configuration for each source is shown in Fig. 8(c).